IEEE Access
Multidisciplinary | Rapid Review | Open Access Journal

Received July 7, 2019, accepted July 19, 2019, date of publication July 23, 2019, date of current version August 9, 2019.

Digital Object Identifier 10.1109/ACCESS.2019.2930623

An Improved VSG Control Strategy Based on the Amplitude-frequency Characteristics of Virtual Power

ZHIJUN LI AND XUEYAN JIA
School of Artificial Intelligence, Hebei University of Technology, Tianjin 300130, China
Corresponding author: Xueyan Jia (summer1903@outlook.com)

This work was supported by the Foundation of the Hebei Province Technology Support Programs of Smart Grid under Grant 15212105.

ABSTRACT There are contradictions between the steady-index and dynamic characteristics of active power responses, when virtual synchronous generator (VSG) is connected to grid as a PQ source. The concept of virtual power was proposed for explaining the physical meaning of the control parameters in this paper. Furthermore, the amplitude–frequency characteristics of virtual power were analyzed and corrected to improve system characteristics, and a general expression of improved VSG control scheme is demonstrated. Afterward, the related control parameters were analyzed and designed for a specific case, and the implement steps were conducted. Finally, the effectiveness of the proposed control method was verified.

INDEX TERMS Virtual synchronous generators (VSG), inertia support power, damping power, amplitude-frequency characteristics, active power oscillation.

I. INTRODUCTION

As the penetration rate of renewable energy increases, the inertia of the power grid decreases. Consequently, the anti-interference and stability of the power system decreases. The randomness and volatility of renewable energy exacerbate this unfavorable situation further. Therefore, the safely and stably operation of power grid is seriously affected [1], [2]. In order to increase the inertia of power grid, VSG control strategy attracts widespread attention. VSG improves the support capability of voltage and frequency effectively by simulating the characteristics of the synchronous generator (SG) [3], [4]. The primary frequency and voltage regulation function are realized by droop control, and the rotor inertia is simulated through virtual inertia link.

The frequency stability can be improved effectively by introducing virtual inertia into the inverter. However, the system damping will reduce and lead to active oscillation. In order to suppress this oscillation, an inertial damping integrated controller is typically formed by introducing damping feedback. When VSG is connected to grid, the frequency support capability and the characteristics of the active power response are determined by the inertia damping characteristics of VSG. As the virtual inertia increases, the frequency support capacity of VSG will be enhanced. However, the overshoot and the adjustment time of the system will be bigger and longer at the same time. The decrease in system damping maybe causes active power oscillation, resulting in DC-side source impact [5], [7]; As the damping increases, the power overshoot will reduce and the effect of system damping will be better. However, a large steady-error will occur in active output power [8], [9].

The inertia damping integrated controller based on PLL (phase-locked loop) is adopted in [10]–[14] to simulate the damping of SG. The damping is proportional to the difference between VSG output voltage angular frequency and grid angular frequency. It is necessary to obtain the grid frequency difference through PLL, because there is not similar physical mechanism that can sense the angular frequency of the rotor. However, the method based on PLL is contrary to the goal of VSG, which makes the inverter to be a self-synchronizing voltage source. The output voltage amplitude and frequency of VSG are controlled independently. At the same time, the introduction of PLL may cause stability problems. In order to avoid the problems caused by PLL, the inertia damping integrated controller without PLL is adapted in [16], [17]. The VSG without PLL simplifies the droop control and damping feedback into a damping link to eliminate the detection of grid frequency. However, the active droop control and damping feedback

The associate editor coordinating the review of this manuscript and approving it for publication was Shravana Musunuri.

are different in control goal. The parameters are designed for active power-frequently droop and active power oscillation may occur. Conversely, the active power-frequently droop characteristics and power distribution may be incorrect [17], [18].

The effects of inertia and damping on the stability were analyzed in [8], [20] when VSG connected to grid. A compromise was made in parameters design between the active power overshoot and adjustment time. However, the contradictions between output active power steady-state and dynamic characteristics have not been regulated. In [21], according to the offset and variation rate of the virtual angular velocity, the bang-bang control strategy was used to change the inertia dynamically. Smaller overshoot and better dynamic characteristics were realized in this method when the index of damping is zero. However, inappropriate selection of the frequency offset threshold causes the value of virtual inertia shaking, resulting in VSG output power and frequency fluctuating. In [22], dynamically damping coefficient was designed to suppress power oscillations. The overshoot of system is reduced but the response speed has some losses. In [22], according to the responses of voltage and frequency in the first oscillation period, the coefficients of inertia and damping are calculated online to eliminate the fluctuation of voltage and frequency. Afterwards, the coefficient of virtual inertia is set to zero, and the damping coefficient is still calculated by the optimization method. However, the optimal method of virtual inertia and damping coefficient is just a compromise of the power overshoot and response speed. The extense of damping coefficient reduces the steady-state power accuracy.

In order to solve the active power responses contradictions between the steady and dynamic characteristics, the concept of virtual power including inertia support power and damping power is proposed in this paper. Furthermore, an improved VSG control strategy is proposed based on the analysis of the amplitude-frequency characteristics of virtual power. According to the demand of the steady and dynamic characteristics, different gains of system in different bands are regulated through inertia damping integrated controller. The closed-loop small-signal transfer function of the improved VSG control strategy is derived in this paper. The effects of the parameters are analyzed, and the parameter design principles of the improved method are given. At last, the improvement control strategy is verified through simulation experiments.

II. VIRTUAL POWER AND PROBLEMS OF ACTIVE OUT POWER RESPONSES

A. THE CONCEPT OF INERTIA SUPPORT POWER AND DAMPING POWER

The control structure of the distributed energy connected to grid through VSG is shown in Fig. 1 [9]. U_{abc} and I_{abc} are the output voltage and current respectively, $P_{r\,ef}$ and Q_{ref} are the given instructions of active and reactive power, Pe and Q_e

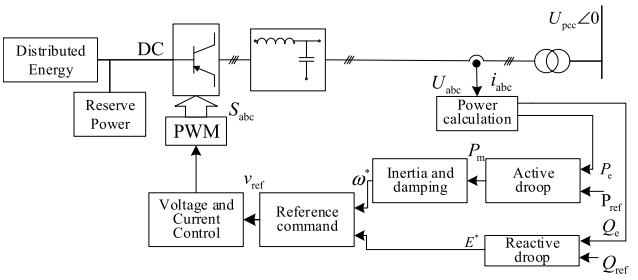

FIGURE 1. Topology of VSG.

are output active and reactive power. P_m is virtual mechanical power, $E*$ and $\omega*$ are voltage and angular frequency reference commands, corresponding to the internal potential and angular frequency of the synchronous machine respectively.

The inputs of the active droop component are the active power command $P_{r\,ef}$ and the active power P_e. The output of this component is the virtual mechanical power P_m, which is consisted of the active power command $P_{r\,ef}$ and the regulated power generated by the virtual governor [24]. This component plays the role of active power-frequency droop and active power reference command.

When working at PQ mode, P_m is expressed as

$$P_m = P_{ref} - K_f(\omega - \omega_0) \tag{1}$$

where P_m, K_f, ω_0 and ω are virtual mechanical power, active power droop coefficient, rated angular frequency and actual output angular frequency.

The inertia damping integrated controller of VSG simulates the rotor motion of SG, and it can be expressed as

$$M\frac{d\omega}{dt} = P_m - P_e - P_D \tag{2}$$

where M is the virtual inertia, $M = J\omega_0$, J is the inertia coefficient. P_D is the damping power, and it can be expressed as

$$P_D = D\omega_0(\omega - \omega_0) = D\omega_0\Delta\omega \tag{3}$$

where D is damping coefficient.

The damping power P_D is proportional to the offset of the angular frequency ω. It can be seen from the formula (1) that the active power droop coefficient K_f has the same expression with the damping coefficient D. In that case, It is possible to analyze D and K_f equivalently through the variation of D.

When the damping coefficient is zero or its effect can be ignored, the formula (2) can be written as

$$M\frac{d\omega}{dt} = P_m - P_e \tag{4}$$

The virtual rotor motion equation is shown in formula (4), where the effect of damping is ignored. P_m usually changes slowly due to the inertia, and it can be seen as approximately constant. From formula (4), the offset of the system frequency is determined by the virtual inertia when the load changes. In other words, a larger virtual inertia lead to stronger frequency support capability.

In order to clarify the concept of inertia support power further, the rotor power equation of VSG can be expressed as formula (5).

$$P_{\mathrm{k}} = \int (P_{\mathrm{m}} - P_{\mathrm{e}})dt = \int J\omega_0 d\omega_0 = \frac{1}{2}J\omega_0^2 \tag{5}$$

Obviously, P_{k} is the kinetic of the virtual rotor. The angular frequency changes with the change of loads, and the offset of the kinetic changed is shown as formula (6).

$$P_J = \Delta P_{\mathrm{k}} = \frac{1}{2}J[(\omega_0 + \Delta\omega)^2 - \omega_0^2] \tag{6}$$

P_J is the inertia support power when the offset of angular frequency occurs.

The system inertia increases due to the introduction of virtual inertia (inertia coefficient). When VSG works at PQ mode, (3) and (6) are substituted into (4), and the small-signal linearization equation of VSG is deducted as

$$P_{\mathrm{D}} = \frac{D(P_{\mathrm{m}} - P_{\mathrm{e}})}{J}\Delta t \tag{7}$$

$$P_J = \frac{(P_{\mathrm{m}} - P_{\mathrm{e}})^2}{2J\omega_0^2}(\Delta t)^2 + (P_{\mathrm{m}} - P_{\mathrm{e}})\Delta t \tag{8}$$

It can be seen from formulas (7) and (8), the inertia support power and the damping power responses have different influence factors and response speeds. As shown in formula (7), when the damping coefficient D increases or the inertia coefficient J decreases, the offset of the damping power P_{D} increases in per unit time. As shown in formula (8), with the increment of inertia coefficient J, the offset of inertia support power P_J decreases in per unit time.

Assuming that the virtual mechanical power P_{m} is constant, it is available from (2), (3), and (6) that

$$\Delta P_{\mathrm{e}} = \Delta P_{\mathrm{J}} + \Delta P_{\mathrm{D}} \tag{9}$$

It can be seen from formula (9), the dynamic characteristics of the output power is determined by the inertia support power and damping power. The inertia support power and the damping power are realized by control system. Therefore, the dynamic responses of virtual power can be adjusted to optimize the output power flexibly.

B. POWER RESPONSE PROBLEM OF CONVENTIONAL VSG

The rotor motion equation control principle of VSG is shown in Fig. 2.

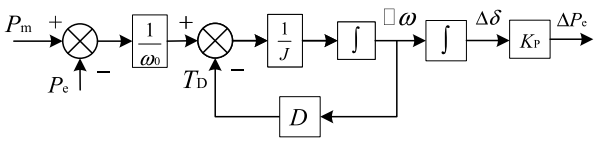

FIGURE 2. Topology of rotor motion equation.

The output power P_{e} can be expressed as

$$P_{\mathrm{e}} = \frac{K_{\mathrm{P}}}{Js^2 + Ds + K_{\mathrm{P}}}P_{\mathrm{m}} + \frac{K_{\mathrm{P}}(J\omega_0 s + D)}{Js^2 + Ds + K_{\mathrm{P}}}(\omega_0 - \omega) = G_{\mathrm{Pe-Pm}}(s)P_{\mathrm{m}} + G_{\mathrm{Pe-}\omega}(s)(\omega_0 - \omega) \tag{10}$$

where $G_{\mathrm{Pe\text{-}Pm}}$ is the transfer function from the virtual mechanical power P_{m} to the output active power Pe; $G_{\mathrm{Pe\text{-}}\omega}$ is the transfer function from the angular frequency to the output active power; K_{P} is the gain coefficient between δ and Pe, $K_{\mathrm{P}} = 3EV/X$ [20], E and V are the terminal voltage and the grid voltage respectively and X is the line impedance.

Available from (7), the output power P_{e} at steady-state can be expressed as

$$P_{\mathrm{e}} = \lim_{s\to 0}[G_{\mathrm{Pe-Pm}}(s)P_{\mathrm{m}} + G_{\mathrm{Pe-}\omega}(s)(\omega_0 - \omega)] = P_{\mathrm{m}} + D(\omega_0 - \omega) \tag{11}$$

As shown in formula (11), there is a steady-error between the steady state output power P_{e} and the expected virtual mechanical power P_{m}, whose magnitude is $D(\omega - \omega 0)$. Obviously, the damping coefficient D should be reduced in the perspective of the steady-error performance.

In Fig. 2, the open loop transfer function of the damping loop is

$$G_{\mathrm{P_D-Pe}}(s) = \frac{\Delta P_{\mathrm{D}}}{\Delta P_{\mathrm{e}}} = \frac{D}{Js} \tag{12}$$

It can be seen from formula (12), the dynamic response of $G_{\mathrm{P_D-Pe}}$ depends on the inertia coefficient J and the damping coefficient D. However, there are mutual constraints in parameter design.

As can be seen from the above analysis, active power steady-error is related to the damping coefficient only. The larger the damping coefficient, the larger the steady-error is. The transient characteristics of active power is related to both the inertia and damping coefficient. From the analysis in part A of Section II, the inertia support power and the damping power have different response speeds and influence factors. There are parameter design contradictions between the dynamic and steady characteristics of the system.

III. IMPROVED VSG CONTROL STRATEGY AND PARAMETER DESIGN

A. AMPLITUDE-FREQUENCY CHARACTERISTICS OF VIRTUAL POWER

The effect of the inertia support power in the conventional VSG can be expressed as

$$G_{\mathrm{J}}(s) = \frac{\Delta\omega}{P_{\mathrm{e}}} = \frac{1}{Js} \tag{13}$$

According to formula (13) and the analysis in part B of Section II, the frequency support capability is enhanced and the frequency responses slower due to the introduction of virtual inertia. As the system damping decreases, the dynamic characteristics will be deteriorated.

In order to overcome this problem, differential element is incorporated into the inertia control channel to improve the transient gain of inertia support power through transient

compensation. The transfer function of the improved inertia channel is shown as

$$G_J(s) = \frac{\omega 0 \Delta\omega}{P_e} = \frac{1}{Js}\left(\frac{Ks}{1+T_1 s} + 1\right) \tag{14}$$

where $T1$ is the high frequency filter time constant, K is the differential coefficient, and $T1 \ll K$.

The bode-plot of the conventional inertia channel and the improved inertia channel with different K are shown in Fig. 3.

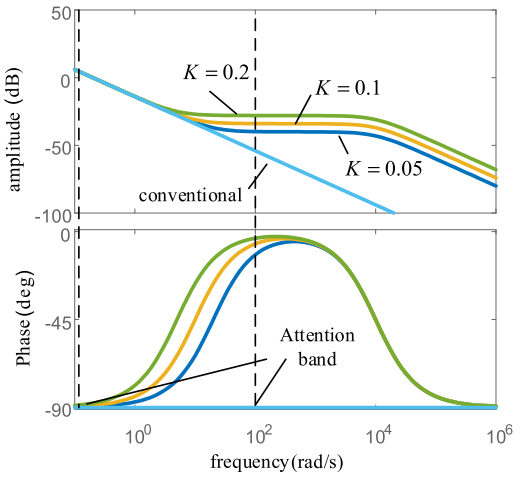

FIGURE 3. Bode-plot of different inertia channel.

It can be seen from the bode-plot in Fig. 3, the improved and conventional inertia channel have the same amplitude-frequency characteristics in the lower frequency band (steady state). As K increases, the transient gain of the improved inertia channel increases, and the bandwidth of transient (transient state) gets wider. Obviously, the system transient gain can be adjusted by the parameter K to meet the requirements of system dynamic performance.

It is worth noting that $T1$ is introduced to reduce high frequency noises, and its effect can be negligible in the frequency band which is concerned in this study.

The damping power in the conventional VSG can be expressed as

$$G_D(s) = \frac{P_D}{\omega 0 \Delta\omega} = D \tag{15}$$

According to formula (15) and the analysis in part B of Section II, as D increases, the system damping effect is better, and a large active power steady-error occurs. Similarly, in order to improve this situation, a similar method can be used to correct the damping channel. It is feasible to reduce the steady-error as much as possible by reducing the steady gain of the damping power. At the same time, the transient gain of system can be maintained to improve its dynamic speed.

the damping power can be rewritten as

$$G_D(s) = \frac{P_D}{\omega 0 \Delta\omega} = \frac{Ds}{1+T_2 s} \tag{16}$$

where T_2 is the transient time coefficient.

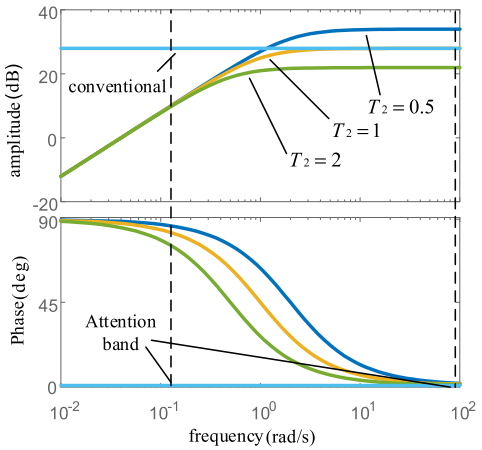

FIGURE 4. Bode-plot of different damping power control channel.

The bode-plot of the conventional and the improved damping channel with different T_2 are shown in Fig. 4.

In the lower frequency band (static state), the improved damping channel reduces the system gain appropriately. The adverse effect of the damping coefficient on the steady-error is weaken. In the higher frequency band (transient), the gains of improved and conventional methods are similar. As the frequency decreases, the transient gain gets larger and the damping capacity increases. In addition, the system response bandwidth can be changed through adjusting $T2$.

B. IMPROVED VSG CONTROL STRATEGY AND PARAMETER ANALYSIS

According to the analysis in part A of Section III, an improved VSG control strategy proposed in this paper is shown as Fig. 5.

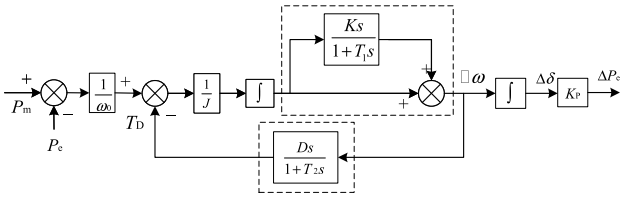

FIGURE 5. Topology of improved VSG.

Where the role of $T1$ is to suppress high frequency noise, $T1 \ll K$, the effect of $T1$ could be ignored in the interested frequency bands.

Obviously, the open loop transfer function of the damping loop is shown as

$$G\mathrm{PD} - \mathrm{Pe}(s) = \frac{\Delta P_D}{\Delta P_e} = \frac{D(1+Ks)}{J(1+T2s)} \tag{17}$$

In contrast with (12), the integral element is substituted by the lead-lag element in the improved VSG control strategy. There are four main parameters in formula (17), namely J, D, $T2$ and K. The steady-state gain of $G\mathrm{PD} - \mathrm{Pe}$ is D/J.

The damping coefficient D and K, the inertia coefficient J and $T2$ are consistent at the respect of system response. Therefore, J and D can be assumed to be fixed, which makes the parameter design easily.

According to the conventional control theory, the n-order lead-lag element will make the design of control system more flexible. The parameters can be designed flexibly according to complex requirements of system performance indexes. In addition, high-order system has advantages of higher control precision and better robustness. Therefore, (17) can be rewritten into a general expression as shown in formula (18), and its control structure is shown in Fig. 6.

$$G_{P_D-P_e}(s) = \frac{\Delta P_D}{\Delta P_e} = C(s),$$
$$C(s) = \frac{D(K_{d1}s+1)(K_{d2}s+1)\cdots(K_{dn}s+1)}{J(T_{d1}s+1)(T_{d2}s+1)\cdots(T_{dn}s+1)} \quad (18)$$

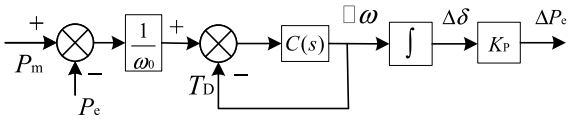

FIGURE 6. Topology of general expression of improved control method.

Theoretically, the n-order lead-lag element can lead to better steady and dynamic characteristics. However, the dynamic performance index analysis will be complicate if there are too many parameters to design. In fact, the closed-loop dominant pole analysis method is used to adopt the n-order to one or two-order element approximately. In order continuing the previous assumptions, the improved damping loop studied in this paper is set to one-order lead-lag element to analyze the influence of numerator indexes and denominator indexes.

According to the amplitude-frequency characteristics analysis of virtual power in part A of Section III, the improved VSG control strategy has been established. The parameters analysis of this method proposed will be developed below.

The closed loop transfer function of the active power is shown as

$$P_e = = \frac{a_1s^2+b_1s+c_1}{as^4+bs^3+cs^2+ds+e}Pr_{ref} + \frac{a_2s^3+b_2s^2+c_2s+d_2}{as^4+bs^3+cs^2+ds+e}(\omega-\omega_0) \quad (19)$$

where,

$$\begin{aligned} a &= JT_1T_2 \\ b &= J(T_1+T_2)+K_fT_1T_2+K_fKT_2+D(T_1+K) \\ c &= J+K_f(T_1+T_2+K)+D+K_PT_2(T_1+K) \\ d &= K_P(T_1+T_2+K)+K_f \\ e &= K_P \\ a_1 &= K_PT_2(T_1+K) \\ b_1 &= K_P(T_1+T_2+K) \\ c_1 &= K_P \\ a_2 &= JT_1T_2 \\ b_2 &= J(T_1+T_2)+K_fT_1T_2+K_fKT_2+D(T_1+K) \\ c_2 &= J+K_f(T_1+T_2+K)+D \\ d_2 &= K_fK_P \end{aligned}$$

where the steady-state active output power can be derived as

$$P_{e\_stac} = \lim_{s\to 0} P_e = \frac{c_1}{e}P_{ref} + \frac{d_2}{e}(\omega-\omega_0) = P_m \quad (20)$$

It can be seen from formula (20) that the steady-state active output power P_e is equal to the virtual mechanical power P_m. The active power steady-error caused by the damping coefficient is eliminated.

Derived from (19), the closed-loop small signal transfer function of active power can be expressed as

$$G_{P_e-P_{ref}}(s) = \frac{P_e}{P_{ref}} = \frac{a1s^2+b1s+c1}{as^4+bs^3+cs^2+ds+e} \quad (21)$$

It can be seen from formula (21) that the improved VSG control strategy adds a pair of closed-loop poles and two zeros generated by the modification of damping power and inertia support power, respectively. The key parameters of inertia support power and damping power are analyzed and designed based on the zero-pole distribution below.

1) PARAMETER ANALYSIS OF IMPROVED INERTIA SUPPORT POWER

Regardless of the effect of the damping channel ($D = 0$), the differential gain K varies from 0 to 1. The system pole-zero map is shown in Fig. 7.

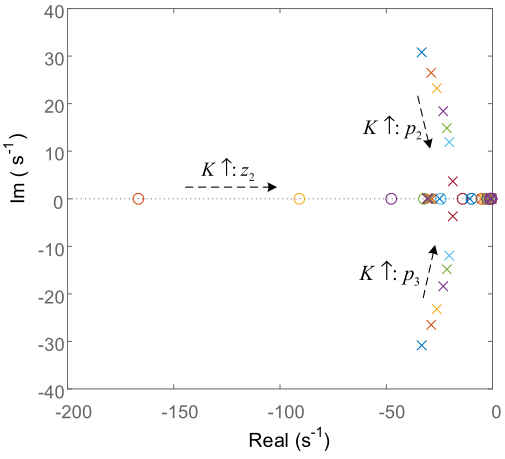

FIGURE 7. Pole-zero map of improved VSG system with different K.

There is a pair of dipoles comprised of pole p_1 and zero z_1. the effects of dipoles on system can be ignored because the position of dipoles hardly move as K varies [28]. The pole p_5 is far away from the imaginary axis, its effect on dynamic of VSG could be ignored. The zero z_2 is far from the imaginary axis when K is zero. As K increases, z_2 approaches the

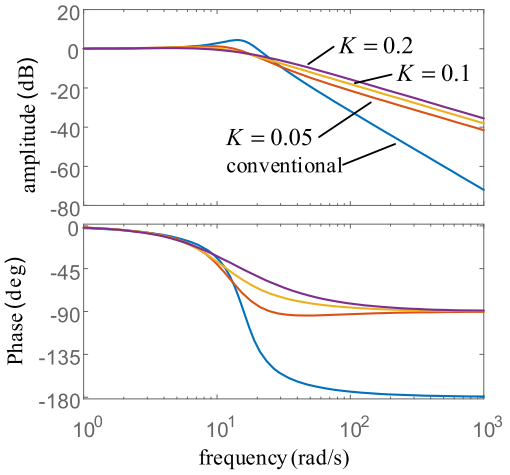

FIGURE 8. The bode-plot of improved VSG control with different K.

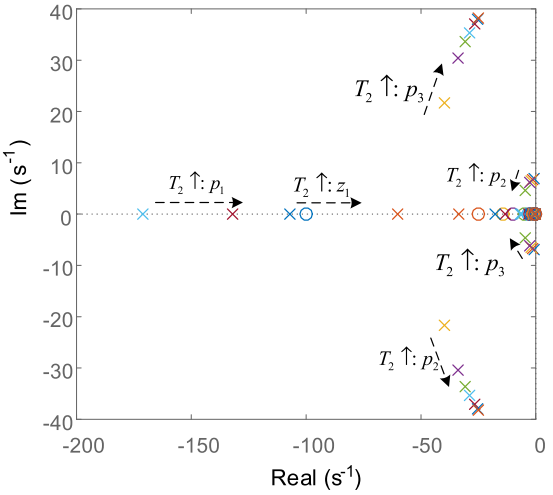

FIGURE 9. Pole-zero map of improved VSG with different T_2.

imaginary axis quickly, and p_2 and p_3 approaches the real axis. As a result, the system damping ratio increases, and the system overshoot decreases. As K continues to increase, the zero z_2 continues moving to the imaginary axis, and p_2 , p_3 meet at the real axis resulting system overdamped. It can be concluded that adjusting the parameters appropriately can improve the system damping ratio and the dynamic responses.

The bode-plot of VSG active power closed-loop transfer function is shown in Fig. 8 when K takes different values.

The amplitude-frequency characteristics using conventional and improved inertia support power control strategy are same in the lower frequency band (steady-state). However, a larger difference appears in the higher frequency band (dynamic). The system gain increases in transient when the improved inertia support power control strategy is used. However, the original gain at steady-state is maintained. A better dynamic response and a less steady-state error are obtained at the same time. Therefore, the dynamic and steady indexes of system can be achieved by optimizing parameter K.

2) PARAMETER ANALYSIS OF IMPROVED DAMPING POWER

Regardless of the effect of the inertia channel (where $K = 0$, $T_1 = 0$), T_2 varies from 0.01 to 5, the zero-pole map of system is shown in Fig. 7.

As shown in Fig.9, the zero-pole variation can be roughly divided into two stages according to the increase of T_2. The pole $p1$ and the zero $z1$ are far away from the imaginary axis when T_2 is very small, which are not appear in Fig. 9. The poles $p2$ and $p3$ are very closed to the imaginary axis. They are system domain poles and are greatly affected by T_2. With the increasing of T_2, the zero $z1$ moves toward the imaginary axis rapidly, and the poles $p2$, $p3$ move to the real axis at the same time, resulting system damping increasing. The two poles meet at the real axis and system over damped at last. As T_2 continues to increase, the pole $p1$ moves to the zero $z1$ in the real axis, forming a pair of dipole. Pole $p2$ and

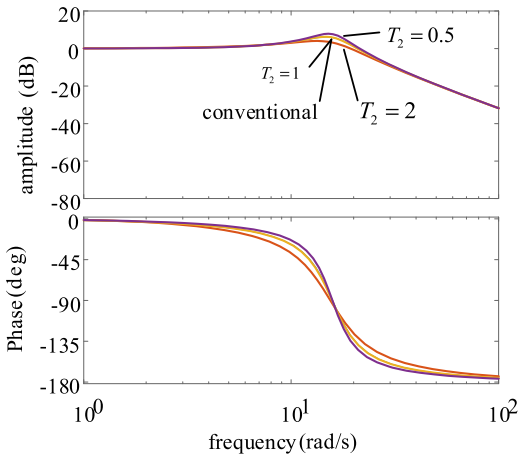

FIGURE 10. System bode-plot of improved VSG with different T_2.

$p3$ meet at the real axes and separate lately, becoming the domain poles. If T_2 increases further, the system damping ratio will decrease. It is not conducive to suppress active power oscillation.

Bode-plot of the system is shown in Figure 10 when T_2 takes different values.

The amplitude-frequency and phase-frequency characteristics curves of improved and conventional VSG control strategy are substantially coincided with each other. The system higher frequency (transient) system gain is reduced when T_2 is greater than 1, and it is improved when less than 1. Therefore, T_2 can be optimized to meet the requirement of system performance indexes.

In order not to change the basic characteristics of conventional VSG, T_2 should be set to appropriate values when poles $p2$ and $p3$ are system domain poles, while the poles are not very closed to the imaginary axis. In that case, the parameters and system performances of VSG can be designed in

a conventional way, reducing the complexity of parameter designing.

3) THE PRINCIPLES OF PARAMETER DESIGN

In the case of Section B in part III, the improved VSG control strategy added a pole and a zero point to system, the bode-plot of system with different control strategy is shown in Figure.11.

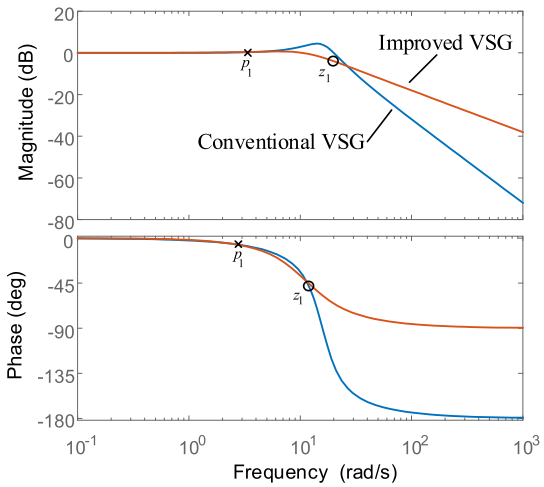

FIGURE 11. Bode-plot of system using different VSG control methods.

It can be seen from the bode-plot in Figure 11, the improved VSG eliminates the resonance peak, and obtains a higher system gain in transient band. The pole point p_1 reduces the system gain in the frequency band of resonance peak, and the zero point z_1 improves the system gains in transient band.

The damping loop of improved VSG is shown in formula (22).

$$C(s) = \frac{D(K_{d1}s+1)(K_{d2}s+1)\cdots(K_{dm}s+1)}{J(T_{d1}s+1)(T_{d2}s+1)\cdots(T_{dn}s+1)} \quad (22)$$

The parameter design principles of improved VSG are conducted as:

Step1) Determine inertia and damping coefficients according to the demand of system through the method of traditional VSG parameter design.

Step2) Choose an appropriate T_{d1} near 1 to suppress resonance peak, in which case the basic characteristics of traditional VSG is not changed.

Step3) Choose K_{dm} which is less than T_{d1} to improve system gain in transient band (m=1, 2, 3 . . .).

Step4) Choose T_{dn} less than T_{d1}, to suppress resonance peak, if not, repeat Step 4 (n=2, 3, 4 . . .).

Step5) repeat Step 3 and Step 4 to meet the demand of system ($n \geq m$) [28].

IV. SIMULATION EXPERIMENTS

The simulations based on Matlab/Simulink are carried out on the single-machine infinite bus system. As shown in Fig.1,

TABLE 1. The parameters of simulation.

parameters	values
Rated power S_b / kW	50
Rated frequency f_b/Hz	50
Rated phase voltage U_n / V	311
LC Filter inductance X_{LC} / mH	1.5
LC Filter capacitor $C_{LC} / \mu F$	600
Line inductance X_L / mH	0.85
Moment of inertia J / Nm	5
Damping coefficient D	25
Differential coefficient K	0.04
High frequency filter time constant T_1 / s	0.0001
Transient time constant T_2 / s	1
Active droop coefficient K_f	25

the default parameters in Tab.1 are used to verify the VSG control strategy proposed in this paper and its parameter characteristics.

A. INFLUENCE OF DAMPING COEFFICIENT ON ACTIVE POWER STEDAY-ERROR

The simulations carried in this section are used to verify the effect of improved damping channel on eliminating the active power steady-state error. There are three experiments carried in this section. The damping coefficient is set to $D = 0$ using conventional VSG control strategy. The damping coefficient is set to $D = K_f$ using conventional VSG control strategy, while the control parameters are set to $D = K_f$, $T_2 = 1$ using improved VSG control strategy.

In this case, the AC grid works at const 380V/50Hz, and the active power reference P_{ref} is 50 kW. Due to the change in the load, the grid frequency is stepped to 50.05 Hz at 3s in the simulation.

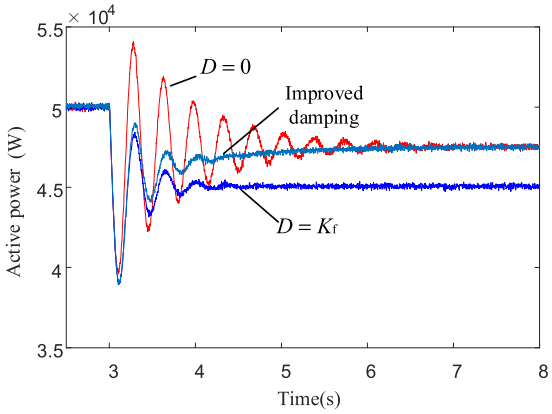

FIGURE 12. The active responses of different damping control strategies.

Using the three groups of control system parameters above, the output active responses are shown in Figure 12, respectively.

Fig.12 shows the results that damping coefficient is set as $D = 0$ and $D = K_f$ separately. When damping coefficient D equals to 0, system damping decreases and power oscillation occurs, causing power impact in the DC-side source. When damping coefficient D equals to K_f, power oscillation is suppressed, yet active power error appears in steady-state. When the improved damping control strategy is used, the power oscillation is suppressed, and there is not active steady-state error. The conclusion can be drawn from the above results, that the active steady-error is eliminated through the improved damping channel effectively. The result of simulation experiments is corresponded with the analysis in part A of Section III

B. INFLUENCE OF CONTROL PARAMETERS ON ACTIVE POWER DYNAMICS

The main parameters of the improved VSG control strategy are T_2 and K according to the discussion above. A group of simulation experiments are carried out to verify the main parameters' influence on active power responses.

In this case, the AC grid works at const 380V/50Hz, and the active power reference P_{ref} is 50 kW. Due to the change in the load, the grid frequency is stepped to 50.05 Hz at 3s in the simulation. The effect of improved inertia channel is out off consider temporarily. T_2 is made some different values respectively in this group of experiments and $D = K_f$.

The active power responses when T_2 takes different values are shown in Fig. 13.

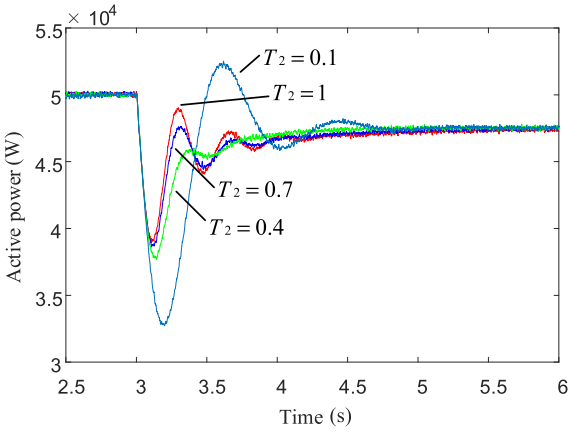

FIGURE 13. The active power responses when T_2 is equal to some different values.

Fig.13 shows the results when T_2 takes different values. When T_2 is in the allowable range, as T_2 decreases, the response speed of system increases and the damping oscillation capability improves. As T_2 further decreases and out of the allowable range, corresponding to the active power response when $T_2 = 0.1$ in Fig.13. In that case, instability appears in active power responses, because the basic control characteristics of the VSG has been changed. Conclusions can be drawn from the simulation experiments results that system damping is enhanced when T_2 takes appropriately values in the allowable range. Once T_2 is out of the allowable range, system instability appears. The conclusions of simulation experiments are consistent with the previous analysis.

In this case, the AC grid works at const 380V/50Hz, and the active power reference P_{ref} is 50 kW. Due to the change in the load, the grid frequency is stepped to 50.05 Hz at 3s in simulation. The parameters of improved damping channel is set as $D = K_f$, $T_2 = 1$. The amplitude-frequency characteristics of conventional and improved VSG control strategy are consistent. K is set to be some different values in this group of experiments.

The active power responses when K takes different values are shown in Fig. 14.

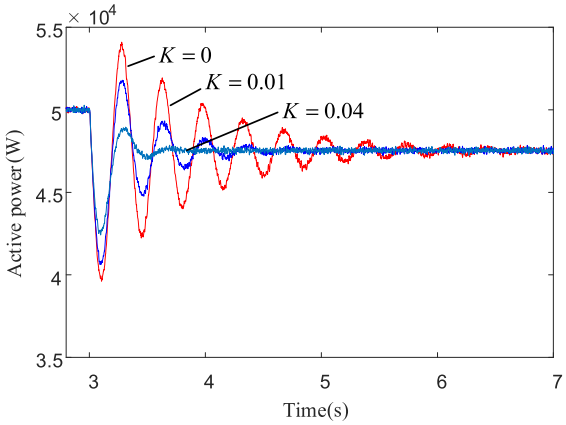

FIGURE 14. The active power responses when K is equal to some different values.

Fig.14 shows the results when K takes different values. When $K = 0$, equals to without additional inertia control, the active power overshoot is about 17.89%, and the adjustment time is about 6.8s. When $K = 0.01$, the active power overshoot is about 13.68%, and the adjustment time is about 4.7s. When $K = 0.04$, the active power overshoot is about 10.50%, and the adjustment time is about 3.8s. The active power overshoot and the adjustment time decreased as K increases. The damping of system increased. The simulation results verify the previous analysis of K.

C. IMPROVED VSG CONTROL STRATEGY

In this case, the AC grid works at const 380V/50Hz, and the active power reference P_{ref} is 50 kW. Due to load changes, the grid frequency is stepped to 50.05 Hz at 3s in the simulation. A group of parameters of improved VSG control strategy are selected according to the analysis and discussions in part A and B of this Section and part A of Section III, that $D = K_f$, $T_2 = 1$, $K = 0.04$. For clearer results, two comparative simulation experiments were carried in this section. The damping coefficient D are set to $D = K_f$ and $D = 0$ respectively using conventional VSG control strategy. The active power responses are shown in Fig.15.

When using the conventional VSG control strategy with the damping coefficient D is set to 0, the active power response

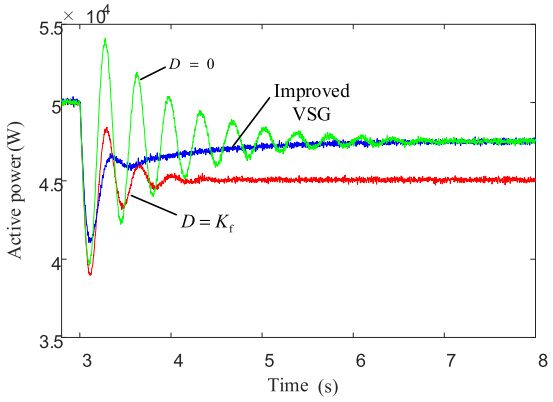

FIGURE 15. The active power responses under different control strategy.

converges slowly with more times of oscillation, and the overshoot is large. When the damping coefficient D is equal to K_f, the times of oscillation is reduced to 3, the convergence accelerates and the overshoot is significantly reduced. However, a large steady-error appears. When the improved VSG control strategy proposed is used, the steady-error caused by the damping coefficient is eliminated, and the active power overshoot and oscillation times are reduced. The dynamic responses of the active power are optimized by this method, reducing the impact on DC-side source effectively which caused by the power oscillations in AC side.

V. CONCLUSION

When VSG is connected to the power grid in PQ mode, the requirements of dynamic and steady characteristics of active power responses are not met at the same time. Concepts of inertia support power and damping power are introduced to analyze the active power response. An improved VSG control strategy is proposed based on the analysis of amplitude-frequency characteristics of virtual power. The gain of system in different frequency bands is altered by the adjustment of inertia and damping integrated controller. Both the dynamic and steady characteristics of the system are met in the improved VSG control strategy.

The following conclusions can be drawn from the analysis and simulation experiments.

1) When VSG is connected to grid at PQ mode, the dynamic and steady characteristics of system are mainly determined by inertia and damping coefficient. There are parameter design contradictions between the dynamic and steady characteristics of active power responses.
2) Different system gains in different frequency bands can be obtained through adding suitable correction to the inertia and damping inertia damping integrated controller (damping loop). Both the dynamic and steady requirements of the VSG can be satisfied.
3) The improved VSG control strategy is more flexible than the traditional way in parameter design. Superior system dynamic and steady quality can be obtained through the design of general expression of improved VSG.

The further work focus on the stability analysis of parallel inverters using improved VSG and the application in micro grid to enhance its stability.

REFERENCES

[1] G. M. Shafiullah, A. M. T. Oo, A. B. M. S. Ali, and P. Wolfs, "Potential challenges of integrating large-scale wind energy into the power grid—A review," *Renew. Sustain. Energy Rev.*, vol. 20, pp. 306–321, Apr. 2013.
[2] C. L. T. Borges and V. F. Martins, "Multistage expansion planning for active distribution networks under demand and distributed generation uncertainties," *Int. J. Elect. Power Energy Syst.*, vol. 36, no. 1, pp. 107–116, 2012.
[3] Q.-C. Zhong, *Power Electronics-Enabled Autonomous Power Systems: Next Generation Smart Grids*. New York, NY, USA: Wiley, 2017.
[4] T. V. Van, K. Visscher, J. Diaz, V. Karapanos, A. Woyte, M. Albu, J. Bozelie, T. Loix, and D. Federenciuc, "Virtual synchronous generator: An element of future grids," in *Proc. IEEE PES Innov. Smart Grid Technol. Conf. Eur. (ISGT)*, Oct. 2010, pp. 1–7.
[5] H. Wu, X. Ruan, D. Yang, X. Chen, W. Zhao, Z. Lv, and Q.-C. Zhong, "Small-signal modeling and parameters design for virtual synchronous generators," *IEEE Trans. Ind. Electron.*, vol. 63, no. 7, pp. 4292–4303, Jul. 2016.
[6] M. A. T. L, L. A. C. Lopes, L. A. M. T, and J. R. E. C, "Self-tuning virtual synchronous machine: A control strategy for energy storage systems to support dynamic frequency control," *IEEE Trans. Energy Convers.*, vol. 29, no. 4, pp. 833–840, Dec. 2014.
[7] G. A. Luders, "Transient stability of multimachine power systems via the direct method of Lyapunov," *IEEE Trans. Power App. Syst.*, vol. PAS-90, no. 1, pp. 23–36, Jan. 1971.
[8] F. Gao and M. R. Iravani, "A control strategy for a distributed generation unit in grid-connected and autonomous modes of operation," *IEEE Trans. Power Del.*, vol. 23, no. 2, pp. 850–859, Apr. 2008.
[9] Q.-C. Zhong and G. Weiss, "Synchronverters: Inverters that mimic synchronous generators," *IEEE Trans. Ind. Electron.*, vol. 58, no. 4, pp. 1259–1267, Apr. 2010.
[10] S. D'Arco, J. A. Suul, and O. B. Fosso, "A virtual synchronous machine implementation for distributed control of power converters in SmartGrids," *Electr. Power Syst. Res.*, vol. 122, no. 6, pp. 180–197, 2015.
[11] H. Alatrash, A. Mensah, E. Mark, G. Haddad, and J. Enslin, "Generator emulation controls for photovoltaic inverters," *IEEE Trans. Smart Grid*, vol. 3, no. 2, pp. 996–1011, Jun. 2012.
[12] J. Liu, Y. Miura, H. Bevrani, and T. Ise, "Enhanced virtual synchronous generator control for parallel inverters in microgrids," *IEEE Trans. Smart Grid*, vol. 8, no. 5, pp. 2268–2277, Sep. 2017.
[13] S. D'Arco and J. A. Suul, "Equivalence of virtual synchronous machines and frequency-droops for converter-based microgrids," *IEEE Trans. Smart Grid*, vol. 5, no. 1, pp. 394–395, Jan. 2014.
[14] T. Shintai, Y. Miura, and T. Ise, "Oscillation damping of a distributed generator using a virtual synchronous generator," *IEEE Trans. Power Del.*, vol. 29, no. 2, pp. 668–676, Apr. 2014.
[15] J. Meng, Y. Wang, X. Shi, C. Fu, and P. Li, "Control strategy and parameter analysis of distributed inverters based on VSG," *Trans. China Electrotech. Soc.*, vol. 29, no. 12, pp. 1–10, 2014.
[16] Z. Lü, W. Sheng, and Q. Zhong, "Virtual synchronous generator and its applications in micro-grid," *Proc. Chin. Soc. Elect. Eng.*, vol. 34, Jun. 2014, pp. 2591–2603,
[17] Q.-C. Zhong, P.-L. Nguyen, Z. Ma, and W. Sheng, "Self-synchronized synchronverters: Inverters without a dedicated synchronization unit," *IEEE Trans. Power Electron.*, vol. 29, no. 2, pp. 617–630, Feb. 2014.
[18] S. Rongliang, Z. Xing, and L. Fang, "Control technologies of multi-energy complementary microgrid operation based on virtual synchronous generator," *Trans. China Electrotech. Soc.*, vol. 31, no. 20, pp. 170–180, 2016.
[19] X. Haizhen, Z. Xing, and L. Fang, "Virtual synchronous generator control strategy based on lead-lag link virtual inertia," *Proc. Chin. Soc. Elect. Eng.*, vol. 37, no. 7, pp. 1918–1926, 2017.

[20] Z. Linn, Y. Miura, and T. Ise, "Power system stabilization control by HVDC with SMES using virtual synchronous generator," *IEEJ J. Ind. Appl.*, vol. 1, no. 2, pp. 102–110, 2012.
[21] J. Alipoor, Y. Miura, and T. Ise, "Power system stabilization using virtual synchronous generator with alternating moment of inertia," *IEEE J. Emerg. Sel. Topics Power Electron.*, vol. 3, no. 2, pp. 451–458, Jun. 2015.
[22] L. Xiong, F. Zhuo, F. Wang, X. Liu, Y. Chen, M. Zhu, and H. Yi, "Static synchronous generator model: A new perspective to investigate dynamic characteristics and stability issues of grid-tied PWM inverter," *IEEE Trans. Power Electron.*, vol. 31, no. 9, pp. 6264–6280, Sep. 2016.
[23] N. Pogaku, M. Prodanovic, and T. C. Green, "Modeling, analysis and testing of autonomous operation of an inverter-based microgrid," *IEEE Trans. Power Electron.*, vol. 22, no. 2, pp. 613–625, Mar. 2007.
[24] J. Liu, Y. Miura, and T. Ise, "Comparison of dynamic characteristics between virtual synchronous generator and droop control in inverter-based distributed generators," *IEEE Trans. Power Electron.*, vol. 31, no. 5, pp. 3600–3611, May 2016.
[25] L. Huang, H. Xin, L. Zhang, Z. Wang, K. Wu, and H. Wang, "Synchronization and frequency regulation of DFIG-based wind turbine generators with synchronized control," *IEEE Trans. Energy Convers.*, vol. 32, no. 3, pp. 1251–1262, Sep. 2017.
[26] D. Chen, Y. Xu, and A. Q. Huang, "Integration of DC microgrids as virtual synchronous machines into the AC grid," *IEEE Trans. Ind. Electron.*, vol. 64, no. 9, pp. 7455–7466, Sep. 2017.
[27] P. Kundur, *Power System Stability And Control*. New York, NY, USA: McGraw-Hill, 1994.
[28] G. F. Franklin, J. D. Powell, and A. Emami-Naeini, *Feedback Control of Dynamic Systems*. Upper Saddle River, NJ, USA: Prentice-Hall, 2005.

ZHIJUN LI received the B.E. degree in automation engineering from the Hebei Institute of Technology, Tianjin, China, in 1986, and the M.E. and Ph.D. degrees in electrical engineering from the Hebei University of Technology, Tianjin, in 2001 and 2004, respectively.

From 1986 to 2012, he was a Research and Development Engineer with Electrical Factory, Hebei University of Technology, where he has been a Professor with Renewable Energy Science and Engineering, since 2013. He has authored over two books and 80 articles. His research interests include power system stability, green energy conversion and control technology, and automatic power generation equipment and its applications.

Prof. Li was a recipient of the Hebei Province Science and Technology Progress Award for two times. He was the Vice Chairman of the Standard Committee for the small hydropower industry of the State Energy Bureau of China. He has participated in the National Key Science and Technology Project.

XUEYAN JIA received the B.E. degree from the Hebei University of Technology, Tianjin, China, in 2017, where he is currently pursuing the M.E. degree. His current research interests include renewable energy generation, microgrid, and stability analysis of inverter-based systems.